Supporting Information for

Do upper-plate material properties or fault frictional properties dominate tsunami earthquake characteristics?

Qingjun Meng[1], Benchun Duan[1*]

(1) Center of Tectonophysics, Department of Geology & Geophysics, Texas A&M University, College Station, TX, United States.

Corresponding author: Benchun Duan (bduan@tamu.edu)

Contents of this file

Figures S1 – S8

Table S1 and S2

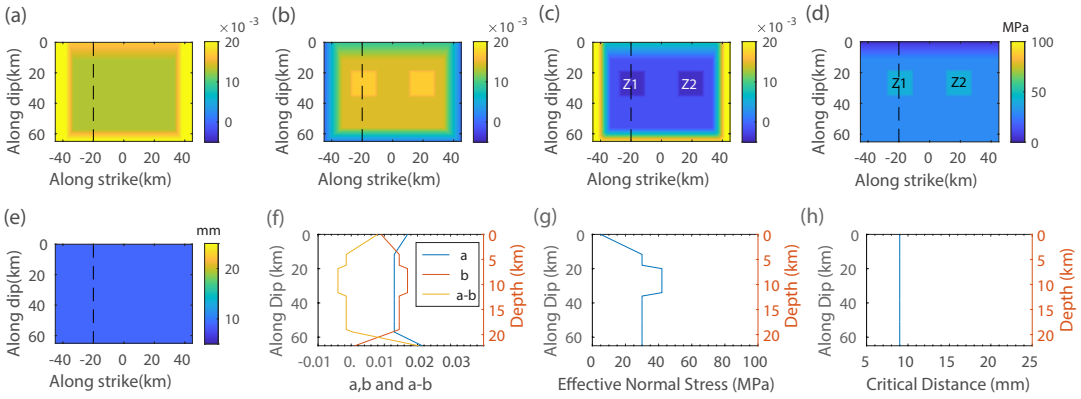

Figure S1. The fault parameters for the nonuniform friction model with low normal stress (in Model 5): distributions of friction parameters (a) *a*, (b) *b*, (c) *a-b*, (d) effective normal stress and (e) critical distance over the fault plane; the cross sections of friction parameters (f) *a*, *b*, *a-b*, (g) effective normal stress, and (h) critical distance along a profile (dashed lines along dip). The *a-b* parameter is the same as shown in Fig. 3. The effective normal stress near trench (depth 0 km) is 5MPa and linearly changes to 30 MPa at depth of 4km and keeps uniform over most of the fault plane, as shown in (g). On asperities Z1 and Z2 normal stress is 42 MPa. Critical distance is 9 mm over most of the fault plane. Compared with the nonuniform friction model shown in Fig. 3, the overall effective normal stress and critical distance is proportionally lower (60%) than that in Model 3 and 4, making the h* unchanged compared with h* in Model 3 and 4, shown in Fig. S3.

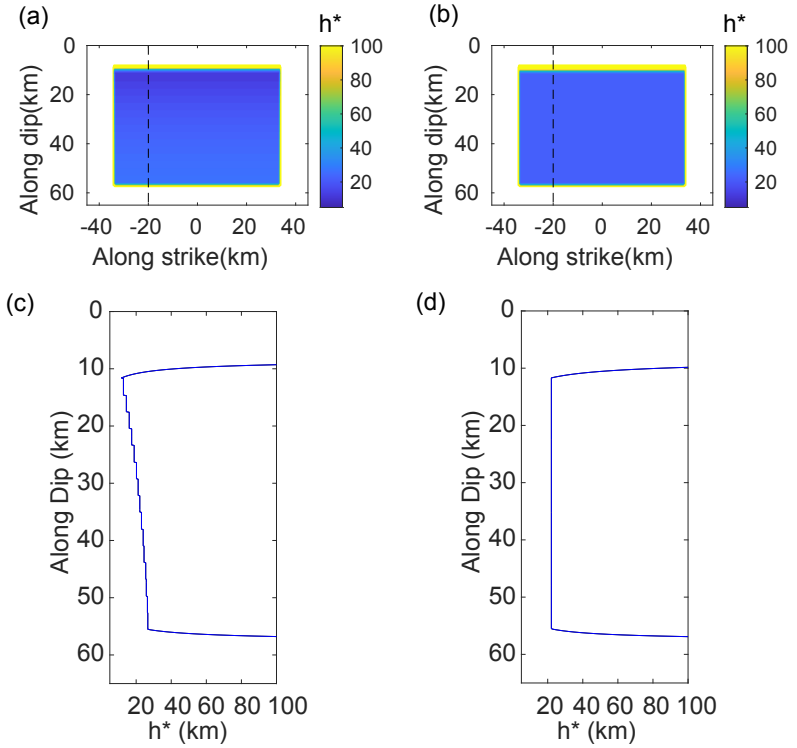

Figure S2. The h* value calculated based on equation (3) for the uniform friction model with (a) depth dependent velocity structure (hanging wall in Model 2), (b) two-layer velocity structure (Model 1 and footwall in Model 2). (c) The h* value along cross section shown by dashed line in (a). (d) The h* value along a cross section shown by dashed line in (b). The area with a-b>0 has no h* value.

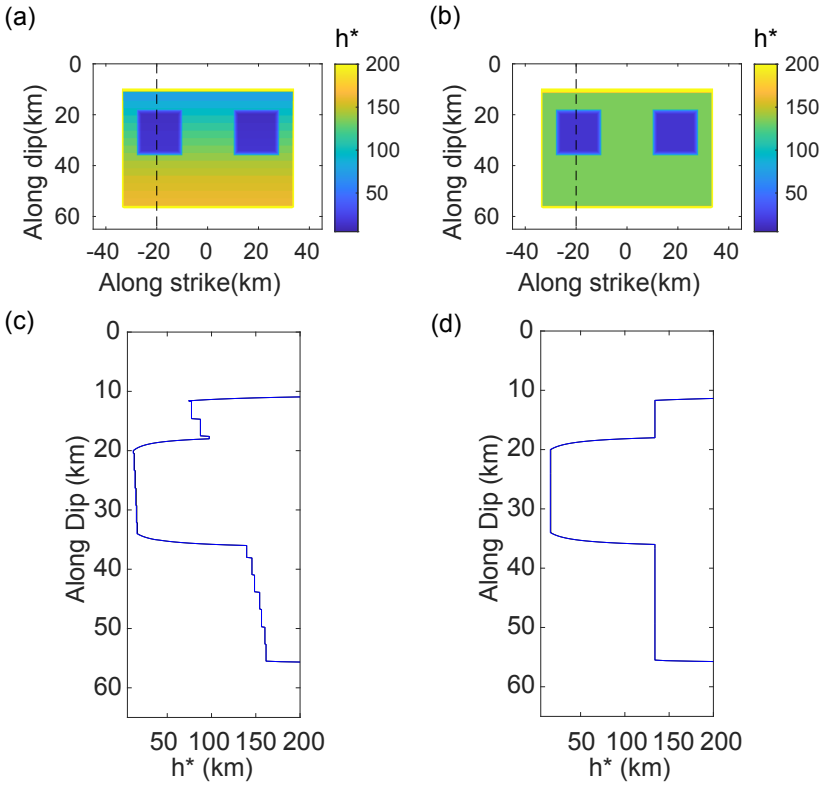

Figure S3. The h* value calculated based on equation (3) for the nonuniform friction model with (a) depth dependent velocity structure (hanging wall in Model 4,5), (b) two-layer velocity structure (Model 3 and footwall in Model 4,5). (c) The h* value along cross section shown by dashed line in (a). (d) The h* value along a cross section shown by dashed line in (b). The area with a-b>0 has no h* value.

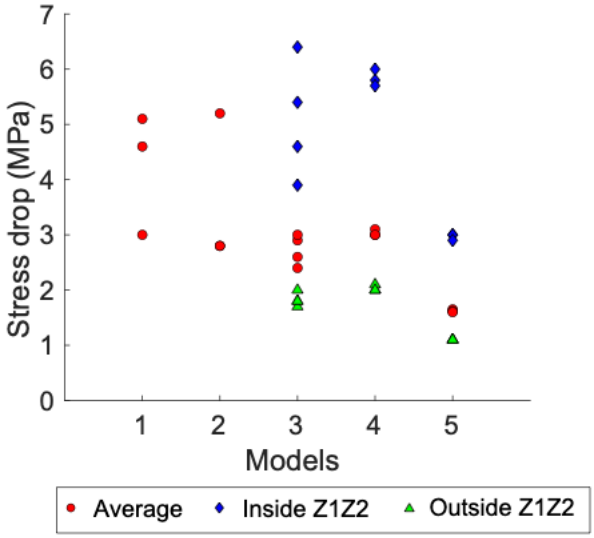

Figure S4. The average stress drop (red dots) over the whole fault plane for dynamic events simulated in Models 1-5. The blue diamonds show average stress drop inside the asperities and the green triangles show the average stress drop outside the asperities for Models 3-5.

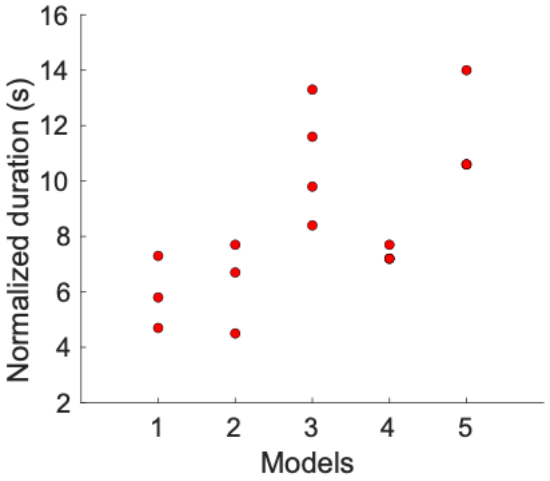

Figure S5. Normalized durations for dynamic events simulated in Models 1-5.

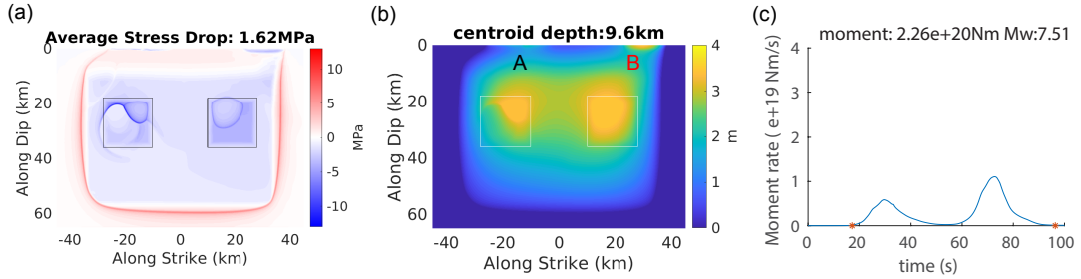

Figure S6. The stress change distribution (a), final slip distribution (b) and moment rate function (c) from dynamic event D2 in Model 5. The white and black boxes show locations of two asperities. Labels A and B in (b) show two large slip areas on the subduction plane near the trench below the two seafloor stations A and B in Fig. 9.

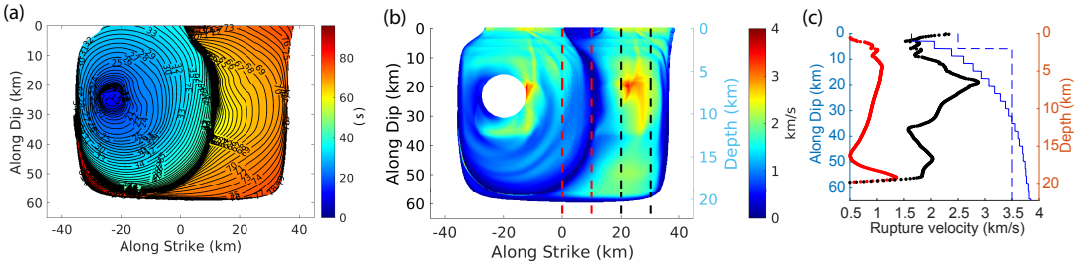

Figure S7. The rupture contours (a), rupture speed distribution (b) and rupture speed profiles (c), from dynamic event D2 in Model 5. In (c), the red velocity profile shows the average rupture speed of each depth over a narrow zone outlined by two dashed red lines in (b), and the black velocity profile corresponds to the average rupture speed within the two black dashed lines in (b). The blue solid line and dashed line represent Vs of the hanging wall and footwall, respectively, for comparison with rupture speed profiles.

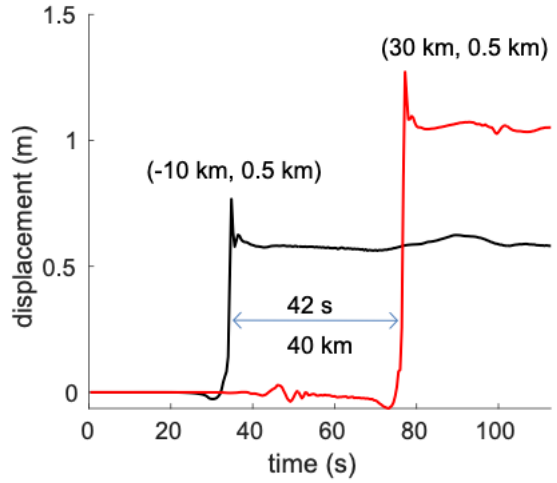

Figure S8. Vertical ground surface displacements for two stations A(black) and B(red), with the

along X (along trench) and along Y (perpendicular with trench) locations illustrated within the parentheses. The same displacement waveforms are marked with same color (black and red) in Fig. 9. The two stations are 40 km away in distance. The sharp increase of waveform amplitudes represents the time when rupture front arrives near two stations (time difference of 42 s).

Table S1. Source parameters for historical tsunami earthquakes.

No.	**Region**	**Date**	**Mw**	**M_0 (Nm)**	**Duration (s)**	**Normalized duration (s)**
1	Japan	1896/06/15	8.0	1.2e21	100	10.1
2	Alaska	1946/04/01	8.2	2.3e21	100-150	10.2
3	Peru	1960/11/20	7.6	3.4e20	125	19.3
4	Peru	1996/02/21	7.5	1.9e20	50	9.4
5	Kuriles	1963/1020	7.8	6.0e20	85	10.8
6	Kuriles	1975/06/10	7.5	2.0e20	80-100	16.6
7	Nicaragua	1992/09/02	7.7	4.2e20	125	18.0
8	Java	1994/06/02	7.6	3.5e20	85	10.2
9	Java	2006/07/17	7.8	6.7e20	185	23.3
10	Mentawai	2010/10/25	7.8	6.7e20	90	11.4

References: 1. Tanioka and Satake, 1996 ; 2. Johnson and Satake, 1997; 3. Pelayo and Wiens, 1990; 4. Ihmlé et al., 1998; 5. and 6. Pelayo and Wiens, 1992; 7. Ihmlé, 1996; 8. Abercrombie et al., 2001; 9. Ammon et al., 2006; 10. Lay et al., 2011

Table S2. Basic model parameters in this study

Parameters	Value
Poisson's ratio ν	0.25
Reference slip velocity V_0	10^{-6} m/s
Steady state friction coefficient f_0	0.6
Loading rate V_{pl}	10^{-9} m/s
Element edge length in x direction Δx	150 m
Fault dipping angle ϕ	20 degrees
Element edge length in y direction Δy	150*cos(ϕ) m
Element edge length in y direction Δz	150*sin(ϕ) m
Time step (dynamic simulation)	0.002 s

References:

Abercrombie, R. E., M. Antolik, K. Felzer, and G. Ekström (2001), The 1994 Java tsunami earthquake: Slip over a subducting seamount, J. Geophys. Res., 106, 6595–6607, doi:10.1029/2000JB900403.

Ammon, C. J., H. Kanamori, T. Lay, and A. A. Velasco (2006), The 17 July 2006 Java tsunami earthquake, Geophys. Res. Lett., 33, L24308, doi:10.1029/2006GL028005.

Ihmle´, P. F. (1996), Frequency-dependent relocation of the 1992 Nicaragua slow earthquake: An empirical Green's function approach, Geophys. J. Int.,127, 75– 85.

Ihmle´, P. F., J. M. Gomez, P. Heinrich, and S. Guibourg (1998), The 1996 Peru tsunamigenic earthquake: Broadband source process, Geophys. Res. Lett., 25, 2691– 2694.

Johnson, J. M., and K. Satake (1997), Estimation of seismic moment and slip distribution of the. April 1, 1946, Aleutian tsunami earthquake, J. Geophys. Res., 102, 11,765– 11,774.

Lay, T., C. J. Ammon, H. Kanamori, Y. Yamazaki, K. F. Cheung, and A. R. Hutko (2011), The 25 October 2010 Mentawai tsunami earthquake (Mw 7.8) and the tsunami hazard presented by shallow megathrust ruptures, Geophys. Res. Lett., 38, L06302, doi:10.1029/2010GL046552.

Pelayo, A. M., and D. A. Wiens (1990), The November 20, 1960 Peru tsunami earthquake: Source mechanism of a slow event, Geophys. Res. Lett., 17, 661– 664.

Pelayo, A. M., and D. A. Wiens (1992), Tsunami earthquakes: Slow thrust-faulting events in the accretionary wedge, J. Geophys. Res., 97, 15,321– 15,337.

Tanioka, Y., and K. Satake (1996), Fault parameters of the 1896 Sanriku tsunami earthquake. estimated from tsunami numerical modeling, Geophys. Res. Lett., 23, 1549–1552.